ACS Chemical Neuroscience

Research Article

pubs.acs.org/chemneuro

Characterization and First Human Investigation of FIBT, a Novel Fluorinated Aβ Plaque Neuroimaging PET Radioligand

Behrooz Hooshyar Yousefi,*[,†,#] André Manook,[†,‡,#] Timo Grimmer,[§] Thomas Arzberger,[∥,⊥] Boris von Reutern,[‡] Gjermund Henriksen,[‡] Alexander Drzezga,[‡] Stefan Förster,[‡] Markus Schwaiger,[‡] and Hans-Jürgen Wester[†]

[†]Department of Pharmaceutical Radiochemistry, [‡]Department of Nuclear Medicine, and [§]Department of Psychiatry and Psychotherapy, Technische Universität München, Munich, Germany

[∥]Centre for Neuropathology and Prion Research and [⊥]Department of Psychiatry and Psychotherapy, Ludwig-Maximilians Universität München, Munich, Germany

Supporting Information

ABSTRACT: Imidazo[2,1-*b*]benzothiazoles (IBTs) are a promising novel class of amyloid positron emission tomography (PET) radiopharmaceuticals for diagnosis of neurodegenerative disorders like Alzheimer's disease (AD). Their good in vivo imaging properties have previously been shown in preclinical studies. Among IBTs, fluorinated [^{18}F]FIBT was selected for further characterization and advancement toward use in humans. [^{18}F]FIBT characteristics were analyzed in relation to Pittsburgh compound B (PiB) as reference ligand. [^{18}F]FIBT and [^{3}H]PiB were coinjected to an APP/PS1 mouse for ex vivo dual-label autoradiographic correlation. Acute dose toxicity of FIBT was examined in two groups of healthy mice. Preexisting in vivo stability and biodistribution studies in mice were complemented with analogous studies in rats. [^{18}F]FIBT was titrated against postmortem human AD brain homogenate in a saturation binding assay previously performed with [^{3}H]PiB. Binding of [^{18}F]FIBT to human AD brain was further analyzed by in vitro incubation of human AD brain sections in comparison to [^{11}C]PiB in relation to standard immunohistochemistry. Finally, [^{18}F]FIBT was administered to two human subjects for a dynamic 90 min PET/MR brain investigation. Ex vivo autoradiography confirmed good uptake of [^{18}F]FIBT to mouse brain and its excellent correlation to [^{3}H]PiB binding. No toxicity of FIBT could be found in mice at a concentration of 33.3 nmol/kg. As in mice, [^{18}F]FIBT was showing high in vivo stability in rats and comparable regional brain biodistribution dynamics to [^{3}H]PiB. Radioligand saturation binding confirmed at least one high-affinity binding component of [^{18}F]FIBT around 1 nM. Good binding of FIBT relative to PiB was further confirmed in binding assays and autoradiographies using post-mortem AD brain. First use of [^{18}F]FIBT in humans successfully yielded clinical [^{18}F]FIBT PET/MR images with very good contrast. In summary, [^{18}F]FIBT has been characterized to be a new lead compound with improved binding characteristics and pharmacokinetics on its own as well as in comparison to PiB. A pilot human PET investigation provided high-quality images with a plausible tracer distribution pattern. Detailed clinical investigations are needed to confirm these first results and to explore the specific qualities of [^{18}F]FIBT PET for dementia imaging in relation to established ligands.

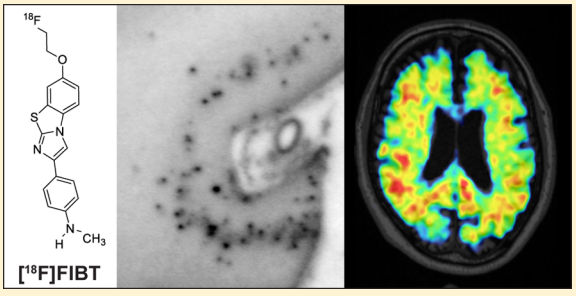

KEYWORDS: *^{18}F-labeled radiopharmaceutical, FIBT, PiB, Alzheimer's disease, PET, amyloid-beta, autoradiography, binding assay*

Amyloid-beta (Aβ) positron emission tomography (PET) began about 15 years ago by exploiting fluorescent dyes already established for in vitro staining of postmortem Alzheimer's disease (AD) tissues as potential in vivo probes.[1] [^{18}F]FDDNP, 1,1-dicyano-2-[6-(dimethylamino) naphthalen-2-yl]propene, was the first ^{18}F-fluorinated dye developed at University of California, Los Angeles in 1999.[2] However, its signal showed considerable nontarget background and relatively low specific binding which resulted in limited further utilization.[3] Shortly after, Pittsburgh compound B or PiB,[4] was developed and has become the most widely clinically used PET tracer for assessment of Aβ depositions in living brain. Moreover, the scientific community currently acknowledges PiB as benchmark amyloid PET imaging agent.

Amyloid-PET has become a noninvasive imaging tool for visualizing and quantifying Aβ deposits, primarily in AD patients. Research on new Aβ tracers was rapidly concentrated on ^{18}F-radiopharmaceuticals with increased sensitivity. Limitations observed with [^{18}F]FDDNP during first clinical studies[3,5] and positive results obtained in IMPY[6] and PiB studies inspired a new series of Aβ ligands, imidazo[2,1-*b*]benzothiazole (IBT),

Received: August 13, 2014
Revised: November 14, 2014
Published: December 8, 2014

DOI: 10.1021/cn5001827
ACS Chem. Neurosci. 2015, 6, 428−437

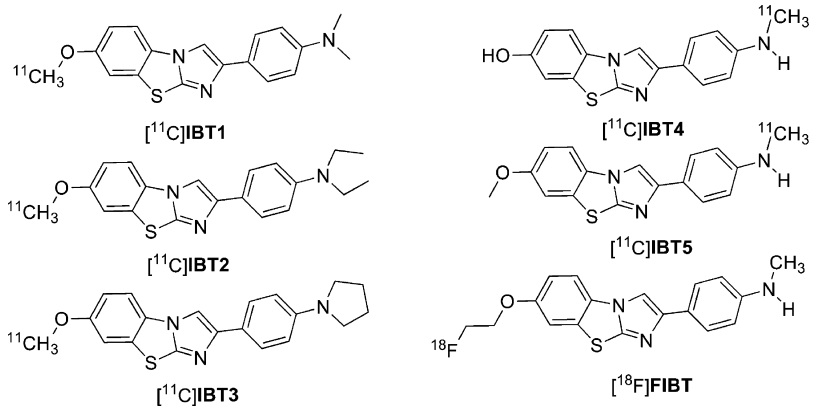

Figure 1. Chemical structures of IBTs (imidazo[2,1-*b*]benzothiazoles) previously investigated[7,8] at preclinical stages.

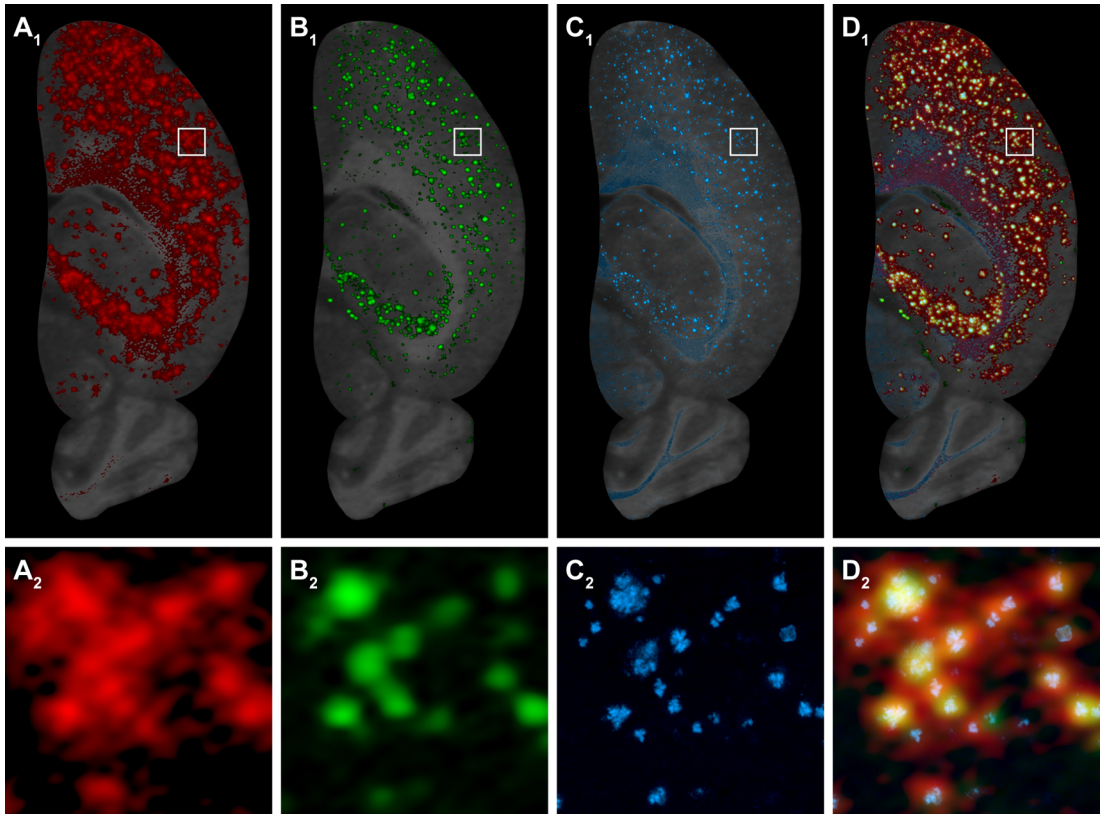

Figure 2. Ex vivo uptake of [^{18}F]FIBT with [^{3}H]PiB in APP/PS1 mouse brain and Thioflavin S binding. Simultaneous dual-label digital ex vivo autoradiography of a 12 μm thick fresh frozen left brain section taken 45 min after coinjecting [^{18}F]FIBT and [^{3}H]PiB to a 12 month old homozygous APP/PS1 mouse and afterward staining the same section with Thioflavin S. (A) [^{18}F]FIBT ex vivo (red). (B) Co-injected [^{3}H]PiB ex vivo (green). (C) Fluorescent Thioflavin S stain of same section presented in panels (A) and (B) (blue). (D) Fusion image of all three signals using only rigid transformations based on optical images. Optical images (gray) as seen in top panels were automatically taken with the digital autoradiograph. In these images, white matter appears in lighter tones of gray. White squares mark areas for magnification as shown in bottom views (A_2)−(D_2).

recently developed in our lab.[7] Selected compounds from this series (Figure 1) succeeded to enter preclinical studies.[7,8] The best ^{18}F-labeled candidate ([^{18}F]FIBT) was selected for further investigations heading toward clinical application.

IBT structural motifs not only share structural features with IMPY but also with PiB: they consist of a planar electron-rich conjugated heteroaromatic system with at least one hydrogen-bond donor and one hydrogen-bond acceptor function. More importantly a phenolic oxygen on IBT is suitable for stable introduction of ^{18}F-fluorine as [^{18}F]fluoroethyl ether by nucleophilic substitution or [^{18}F]fluoroethylation to create [^{18}F]FIBT.[8]

Previously, we reported high binding affinities of FIBT to synthetic Aβ aggregates (K_i = 2 nM for Aβ_{1-40} and K_i = 3 nM for Aβ_{1-42}), its suitable lipophilicity (log P = 1.9) and good initial brain uptake and desirable pharmacokinetics in Balb-C mice.[8] FIBT demonstrated good in vivo stability in mice, excellent brain penetration and suitable washout and high-contrast PET imaging in APP/PS1 mice. Furthermore, high binding selectivity of FIBT for Aβ (>300-fold) versus recombinant tau ($K_i \gg 1000$ nM) and α-synuclein aggregates ($K_i \gg 1000$ nM) were documented. This

DOI: 10.1021/cn5001827
ACS Chem. Neurosci. 2015, 6, 428−437

indicated that FIBT shows no significant binding to these targets (data not shown) and may hence act as a 'pure' Aβ binding radiopharmaceutical.

A previous publication[8] on [18F]FIBT presented fundamental in vitro data as well as first ex vivo and in vivo preclinical data in transgenic and control mice including successful proof-of-principle small-animal PET. In the current study, we have continued our investigation of [18F]FIBT characteristics by further preclinical ex vivo studies in APP/PS1 mice and in vivo toxicity examinations in healthy mice. Our previous in vivo stability study in mice[8] has been complemented here in an analogous experiment in rats. Analyses included [18F]FIBT saturation binding assays using human AD brain tissue (employing a protocol previously established with [3H]PiB[9]) as well as in vitro autoradiography and its correlation to [11C]PiB binding and conventional immunohistochemistry. The study closes with the presentation of the first human [18F]FIBT PET image data.

RESULTS AND DISCUSSION

After two decades of research and development in diagnostic Aβ radiopharmaceuticals, there are ever growing international industrial and academic research endeavors toward new lead structures with better Aβ (and τ and α-synuclein) binding characteristics and brain pharmacokinetics hoping to improve diagnostics at earlier stages of neurodegenerative diseases leading to dementia. Previously, we have shown the good imaging potential of a newly developed class of Aβ tracers called imidazo[2,1-*b*]benzothiazoles (IBTs). Among these, [18F]FIBT is a novel 18F-fluorinated IBT-derivative with reported favorable in vitro, ex vivo, and preclinical in vivo characteristics. This report supports these first findings and further presents the first imaging results of its use in human subjects with cognitive complaints.

Diagnosis of dementia has never been trivial but becomes ever more challenging as different types of intra- and extracellular neuropathological protein aggregates seen on microscopic level show more overlap than previously known.[10] In the beginnings, the term "Amyloid-PET" was used in analogy to PET for imaging Aβ in AD. Today, "Amyloid-PET" needs to be taken literally, and the imaging community is on the verge of talking about "Tau-PET" and maybe soon "Synuclein-PET".

Development of next-generation ligands for improved diagnosis of different neurodegenerative diseases leading to dementia is already in progress. Clinicians and researchers ask for better pharmacokinetics and pharmacodynamics and improved binding behavior and specificities to yield stronger signals and better image contrast for various neuropathological protein aggregates. One idea behind is that higher binding affinities may increase imaging sensitivity and hence enable earlier diagnosis of disease.

[18F]FIBT may be such a next-generation ligand. Its high exclusive specificity for Aβ as described in the introduction make it a "pure" Aβ radiopharmaceutical, while its general characterization results presented in this study prove it to be competitive to existing Aβ ligands.

Ex Vivo Autoradiography with APP/PS1 Mouse Brain. Preclinical PET imaging with [18F]FIBT has previously been performed in an APP/PS1 mouse model of AD.[8] This mouse has profoundly been characterized in general[11] as well as for PET imaging purposes[9,12] using the reference ligand PiB. The multimodal evaluations in this mouse model[9] may serve as a reference database for the characterization of novel ligands like [18F]FIBT.

To build a bridge from preclinical to clinical studies and from rodent brain material to human brain material, [18F]FIBT was coinjected with [3H]PiB in an APP/PS1 mouse to verify [18F]FIBT uptake to Aβ plaques in relation to PiB and Thioflavin S on the same mouse brain section. Figure 2 shows the trimodal imaging result of this coinjection with fluorescent counterstain. Previous results with PiB and Thioflavin S in this mouse[9] were reproduced and created a reference for simultaneous [18F]FIBT binding. [18F]FIBT clearly showed strong uptake and an identical pattern with the other two Aβ ligands as can best be observed in panel D_2 of Figure 2. Signal in white matter was strongest in Thioflavin S fluorescence.

To link this work to the first publication of [18F]FIBT and to stay consistent with our protocols that use PiB as reference wherever possible, [18F]FIBT was coinjected with [3H]PiB to an APP/PS1 transgenic mouse for simultaneous dual-label digital ex vivo autoradiography followed by Thioflavin S staining of the same section used for autoradiography. The applied mouse line was profoundly characterized in general[11] as well as for imaging with PiB[9] to create a reference for evaluation of novel imaging markers like the IBTs.[7,8] Results presented in Figure 2 confirmed the good in vivo passing of [18F]FIBT across the blood-brain barrier and its nearly identical uptake to Aβ plaques in comparison to [3H]PiB and Thioflavin S. The higher resolution of [3H]PiB signal in this method is related to its label. White matter retention of fluorinated Aβ radiopharmaceuticals is a well-known phenomenon and Figure 2 shows that to a degree [18F]FIBT is also taken up in white matter of mouse brain. Interestingly, Thioflavin S fluorescence in rodent white matter appears to be at least equally strong. Figure 2 showed strong consistency of FIBT and PiB binding on rodent brain material and built a bridge to Figure 5 which reports similar results using human brain sections.

Single-Dose Toxicity in Mice. A small toxicity study is shown in context of first use of FIBT in humans and in an understanding that it merely provides first basic orientation. The choice of single-dose concentration of 33.3 nmol/kg body weight relates to a specific activity of 37 GBq/mmol after end of radiosynthesis. Common range of achievable specific activities during 18F-labeling in our lab is between 18 and 74 TBq/mmol which means that simulating a specific activity of 37 GBq/mmol for toxicity corresponds to an FIBT concentration that is about 1000 times higher than usual correlating to a failure or at least worst-case scenario during radiosynthesis. The results from this single-dose acute intravenous toxicity study imply that the median lethal dose (LD_{50}) of FIBT after intravenous bolus injection to female mice must be substantially higher than 33.3 nmol of FIBT per kilogram body weight as there were absolutely no signs of toxicity at this concentration.

To prepare use in humans and to mimic a worst possible radiolabeling situation, a single-dose acute intravenous study in two groups of healthy female mice was performed. Observational period after bolus injection of 33.3 nmol FIBT per kilogram body weight was 14 days. All animals stayed healthy and remained normal during the course of the study. A single animal lost 7% of body weight during first week after treatment but recovered in the second week after treatment. The body weight of all other animals was within the range commonly recorded for this strain and age. No macroscopic findings were recorded at necropsy. All animals survived treatment without showing any clinical signs of toxicity.

In Vivo Stability and Regional Brain Biodistribution in Rats. The first report on [18F]FIBT presented in vivo stability

DOI: 10.1021/cn5001827
ACS Chem. Neurosci. 2015, 6, 428−437

data in blood and brain at 10 and 30 min time points yielded in mice[8] in relation to [3H]PiB. Here, we additionally show [18F]FIBT stability in rats relative to [3H]PiB including later time-points corresponding to the larger rodent organism. Results confirmed the same principle behavior in male Swiss-Webster rats as in male Balb-C mice.

Table 1 describes that [18F]FIBT in vivo stability was nearly equal to [3H]PiB in blood and brain of rats. The fraction of intact [18F]FIBT in rat brain after 90 min still is higher than 70%. The same experiment yielded regional [18F]FIBT brain biodistribution data for individually dissected brain regions (Figure 3) to describe [18F]FIBT uptake kinetics in various parts of the rat brain relative to cerebellum. A similar experiment was performed for [3H]PiB at 30 min p.i. in 9 month old female C57BL/6J mice previously.[9] Data are included in Figure 3 for better reference.

Table 1. In Vivo Stability of [18F]FIBT in Brain and Blood of Rats (% Intact Tracer)[a]

	[18F]FIBT		[3H]PiB	
time after injection	brain	blood	brain	blood
2 min	104 ± 5		101 ± 4	
30 min	89 ± 5	65 ± 4	92 ± 3	67 ± 2
90 min	71 ± 3	37 ± 13	74 ± 2	41 ± 6

[a]Fraction of intact [18F]FIBT in % at 2 min, 30, and 90 min p.i. in relation to [3H]PiB as measured by their radioactivity in blood and brain of male Swiss-Webster rats. Number of animals per time point and tracer was $N = 3$. Error measures indicate standard deviation.

Brain biodistribution data showed lower uptake (ratios < 1) of and faster washout in cortical and central (nontarget containing) brain structures than in cerebellum. Exceptions were diencephalon and midbrain with slightly higher tracer uptake than cerebellum and olfactory system with possible signs of tracer drainage revealing at the later 90 min time-point. In general, all of these observations were in full correspondence to and in similar ranges like [11C]PiB distribution in control mice.

All in vivo stability and pharmacokinetic data retrieved from rats were in full correspondence to what was previously published for [18F]FIBT and [11C]PiB in mice.[8,9] In rats, metabolism of FIBT in blood and brain seemed comparable to PiB (Table 1). Previously, blood metabolism of FIBT in mice had been slightly higher than PiB[8] suggesting that FIBT in blood of mice was metabolized slightly faster than PiB.

Also, regional dynamic [18F]FIBT brain biodistribution in rats expressed a similar behavior to regional [11C]PiB brain biodistribution in mice. [18F]FIBT shared reversed uptake behavior (region-to-cerebellum ratios <1) with [11C]PiB for tissues without target probably due to white matter binding in cerebellum as previously postulated.[9] The similarly reversed uptake of [18F]FIBT and [11C]PiB supports the claim of relatively low white matter binding of [18F]FIBT as already shown in ex vivo autoradiography with both tracers (Figure 2). There was no such reversal for midbrain structures. The same phenomenon had previously been shown for [11C]PiB and was independently confirmed[9] in histology quantifications with Thioflavin S. In the same way, trapping signs for [18F]FIBT in olfactory system of rats correspond to results for [11C]PiB in mice which is most likely related to excretion pathways for cerebrospinal fluid to nasal lymphatics.[13]

Radioligand Saturation Binding to Human AD Brain Homogenates. In vitro tracer binding is a sensitive reference for in vivo PET binding of the ligand.[14] [18F]FIBT was titrated against a postmortem human AD homogenate which had previously been used for in vitro [3H]PiB binding,[9] thus yielding

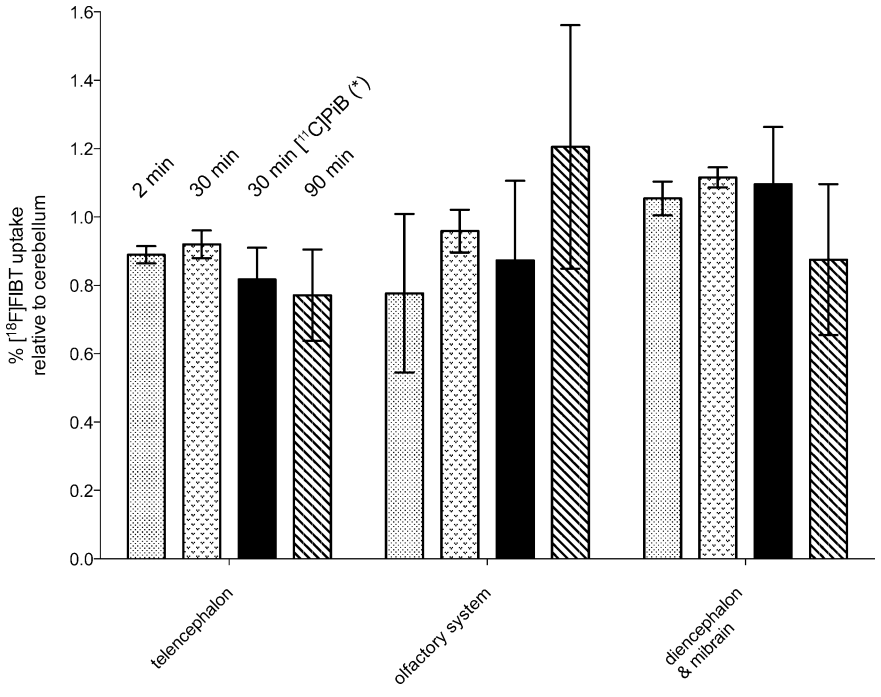

Figure 3. Regional [18F]FIBT brain biodistribution in rats. Uptake kinetics of [18F]FIBT in three brain regions (telencephalon, olfactory system, and diencephalon with midbrain) of male Swiss-Webster rats as measured after dissection and individual counting in % ID/g relative to cerebellum. Individual bars per brain region show 2, 30, and 90 min time points after injection ($N = 3$ for each time point). Already published data for [11C]PiB at 30 min p.i. in 9 month old female C57BL/6J mice ($N = 5$) yielded with the same method[9] are included as reference (black bars). Error bars indicate standard deviation.

DOI: 10.1021/cn5001827
ACS Chem. Neurosci. 2015, 6, 428−437

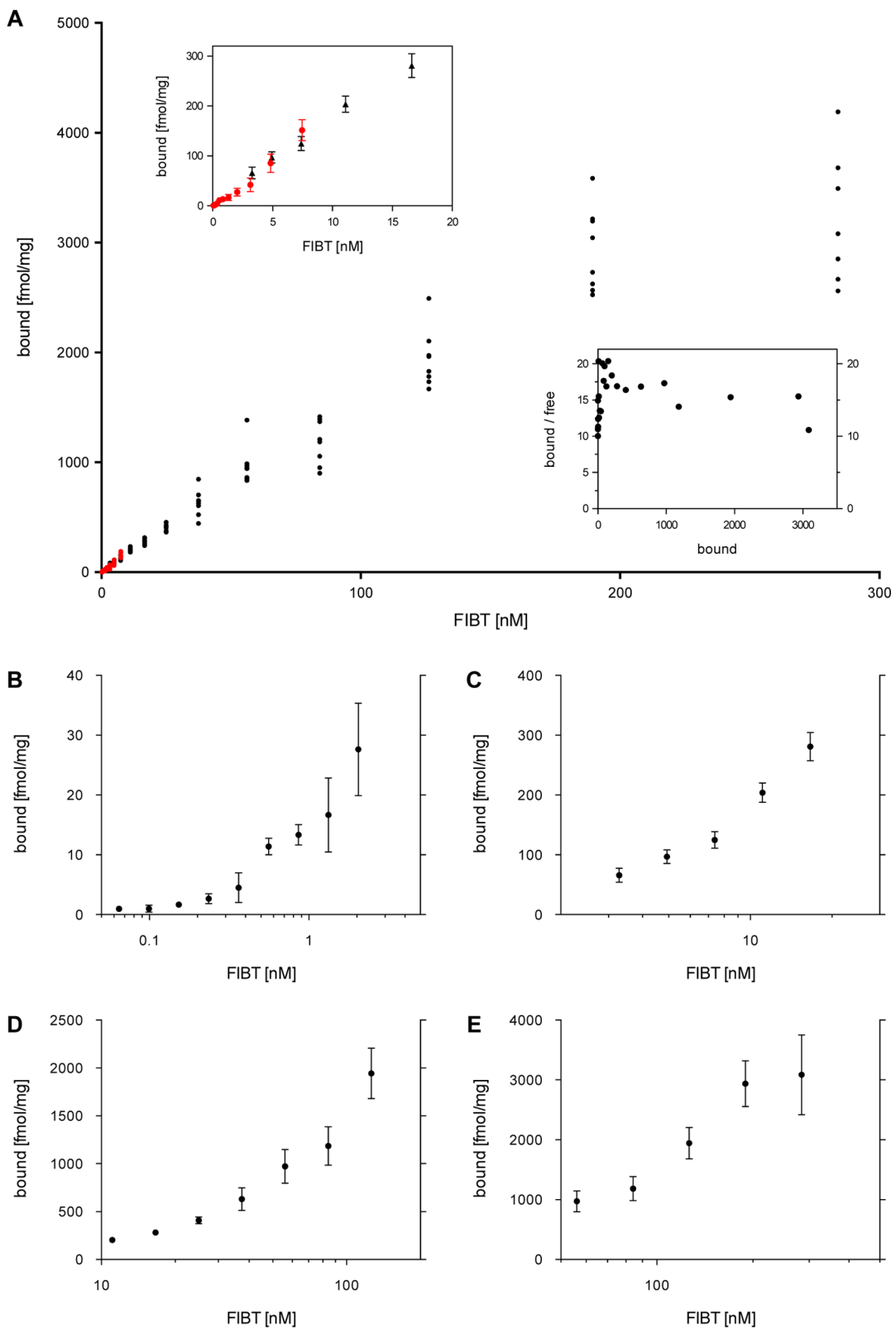

Figure 4. In vitro binding assay with [^{18}F]FIBT to human AD brain homogenates. Specific [^{18}F]FIBT saturation binding to same human AD brain homogenate as previously used for [^{3}H]PiB binding.[9] (A) Full data set of two binding experiments with [^{18}F]FIBT to human AD tissue containing Aβ deposits at low and high concentrations showing data octuples per concentration. Inset top left depicts how the two data sets (separated in red and black color) fit together. Inset bottom right shows the full data set transformed to a Scatchard plot. (B–E) Semilogarithmic representation of specific binding data at different concentration ranges of the binding data set shown in panel (A) as a way of magnification and to delineate inflection points. Panels (B) and (E) present most obvious inflection points related to dissociation constants around 1 nM (panel (B)) and 300 nM (panel (E)) reflecting the principle Scatchard plot behavior shown in right inset of panel (A). For this, also see Supporting Information Figure 1. Wherever shown, error bars indicate standard deviations.

DOI: 10.1021/cn5001827
ACS Chem. Neurosci. 2015, 6, 428–437

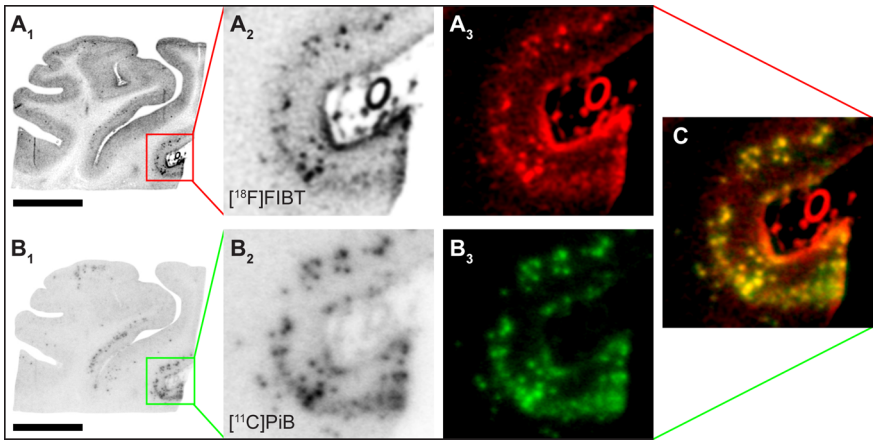

Figure 5. In vitro autoradiographs showing [^{18}F]FIBT uptake in relation to [^{11}C]PiB binding on human AD brain sections. In vitro [^{18}F]FIBT autoradiography following [^{11}C]PiB autoradiography using the same human brain section of 5 μm thickness from a 84 year old male Alzheimer patient. (B_{1-3}) First, a freshly deparaffinized section was incubated with [^{11}C]PiB to guarantee best possible binding of the reference ligand. (A_{1-3}) After [^{11}C]PiB autoradiography, the same section was reused for [^{18}F]FIBT incubation. Overviews of FIBT (panel A_1) and PiB (panel B_1) autoradiographs show a similar uptake pattern on the brain section. Red (FIBT) and green (PiB) colored squares indicate areas for magnification as presented in panels A_{2-3} for FIBT and panels B_{2-3} for PiB. (C) Fusion of both modalities. Plate scanning resolution is 25 μm. Black color bar represents 1 cm.

direct comparability between these two Aβ radiopharmaceuticals. A broad range of tracer concentrations was covered (0.06−284 nM) in two sets of experiments which fitted well together after transforming units to tracer concentration per tissue mass (Figure 4A, left inset). Figure 4A provides an overview of all specific binding replicates of this study.

Tracer concentrations spread over four magnitudes and required magnification of tracer ranges for better visibility of possible binding site behavior (Figure 4B−E). For magnified views, concentration axes were plotted logarithmically to visibly perceive possible inflection points and plateaus. Four concentration ranges were identified to contain inflection points and plateaus. The Scatchard plot in the right inset of Figure 4A as well as panel (B) of the same figure indicated the presence of a binding site around 1 nM while panel (E) delineated the lowest affinity binding site measured in this study. Supporting Information Figure 1 presents more detailed views of these graphs and a comparative theoretical binding curve simulation in order to further address the high-affinity binding site.

It is noteworthy that the same experimental setup used for radioligand saturation binding had been applied for previous work with [^{3}H]PiB and yielded very robust and accurate data.[9] The protocol was just slightly adapted to the change of label. Furthermore and most important for this study in relation to PiB, the same human AD brain homogenate was used as for the [^{3}H]PiB binding study to enable best comparison (without any freeze−thaw cycles in between). Similar to considerations for the toxicity study, ligand concentrations were calculated according to worst estimates for specific activity of each synthesis (18 TBq/mmol). To cover a broad range of concentrations, data of two experiments were put together. The feasibility of this approach, that is, overlapping concentration ranges fitting together well, also confirmed the robustness of the experimental setup (Figure 4).

There were notable differences in radioligand binding to the same human AD brain homogenate between [^{3}H]PiB and [^{18}F]FIBT. The most obvious difference was a clear one-site saturation binding behavior of PiB[9] with relatively early saturation around 10 nM while FIBT seemed to reach various plateaus with an apparent final saturation toward 300 nM. It is this difference in binding behavior that would require simultaneous parameter fitting of multiple invariant binding sites located close to each other in their concentrations. This causes considerable challenges in mathematical modeling of the binding data. Hence, this study focuses on displaying the experimental data (Figure 4) for the experienced reader in addition to theoretical binding curve simulations (Supporting Information Figure 1). Looking at the beginnings and ends of the experimental binding curves (Figure 4B, Supporting Information Figure $1A_2$ and B) enables observation of at least one high-affinity and one low-affinity binding site component with the high-affinity binding site located around 1 nM. This in vitro data confirmed [^{18}F]FIBT to possess preferable binding characteristics as a PET ligand as had already been suggested by successful preclinical PET in mice[8] and as was shown with first clinical PET in this study (Figure 7) as well.

In Vitro Autoradiography of Human AD Brain. *FIBT in Relation to PiB.* In analogy to digital ex vivo dual-label autoradiography with [^{18}F]FIBT and [^{3}H]PiB (see Figure 2), conventional in vitro autoradiographs were taken after sequential [^{11}C]PiB and [^{18}F]FIBT incubation on the same human AD brain section (Figure 5). [^{11}C]PiB was used first (Figure 5B) to guarantee best possible binding results of the reference ligand.

Similar to ex vivo autoradiography with APP/PS1 mouse brain, in vitro autoradiographs with human AD brain show identical patterns of [^{18}F]FIBT uptake to Aβ plaque structures in relation to [^{11}C]PiB.

To complete the description of [^{18}F]FIBT binding behavior to human AD brain material and to provide a correlation between [^{18}F]FIBT binding on mouse and human brain tissue, human AD brain sections were incubated with [^{18}F]FIBT in relation to [^{11}C]PiB and conventional immunohistochemistry for Aβ and τ on the same sections. [^{11}C]PiB was used first to guarantee that binding of PiB as positive reference ligand would be optimal. Similar to ex vivo results in mouse brain (Figure 2), the uptake pattern as shown in conventional plate autoradiographs (Figure 5) delineated nearly identical uptake patterns of both ligands. Figure $5A_{2-4}$ shows how [^{18}F]FIBT also bound to the section rim and the subarachnoid vessel in the center of magnified views (red colored only in fusion Figure 5C). This binding is probably method-related, as there is no relevant Aβ present in these structures as shown in 4G8 stains in Figure 6A.

DOI: 10.1021/cn5001827
ACS Chem. Neurosci. 2015, 6, 428−437

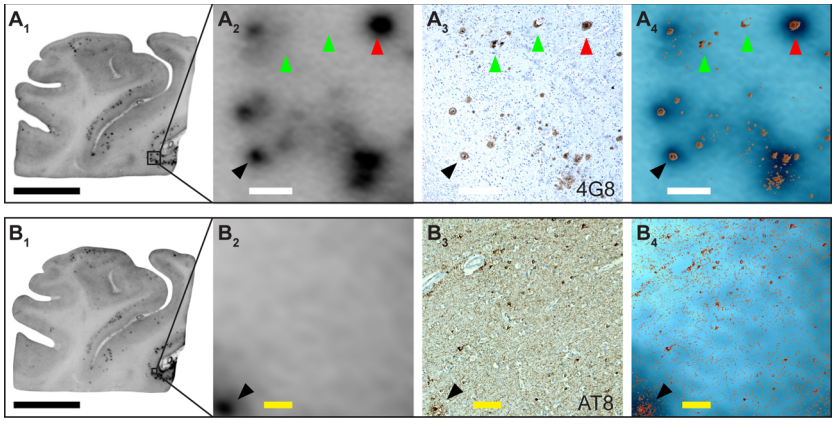

Figure 6. In vitro [^{18}F]FIBT autoradiography in relation to amyloid and tau immunohistochemistry. In vitro [^{18}F]FIBT autoradiography on consecutive (A_1 and B_1) human brain sections of 5 μm thickness from a 84 year old male Alzheimer patient (neighboring section presented in Figure 5). Following autoradiography, brain sections were stained with 4G8 (A_{3-4}) and AT8 (B_{3-4}) monoclonal antibodies for conventional immunohistochemistry. Micrographs were rigidly transformed for coregistration with autoradiographs. Panel (A_4) shows that [^{18}F]FIBT uptake was always 4G8-positive and correlated to Aβ plaque density, showing a strong signal for compact plaques (red arrowhead) and cored plaques (black arrowhead) but a faint or no signal for less compact or diffuse or perivascular plaques (green arrowheads). Panel (B_4) marks a large field of τ tangles and confirms that [^{18}F]FIBT does not bind to τ. As reference, left bottom corner shows a neuritic (i.e., τ-containing) dense core amyloid plaque (black arrowhead) with [^{18}F]FIBT retention. For larger field views of panels (A_4) and (B_4), see Supporting Information Figure 2. Black squares in left column (A_1 and B_1) indicate magnification as shown in columns 2−4. Plate scanning resolution for autoradiographs is 25 μm. Black color bar represents 1 cm, white bar 1 mm, and yellow bar 100 μm in reality.

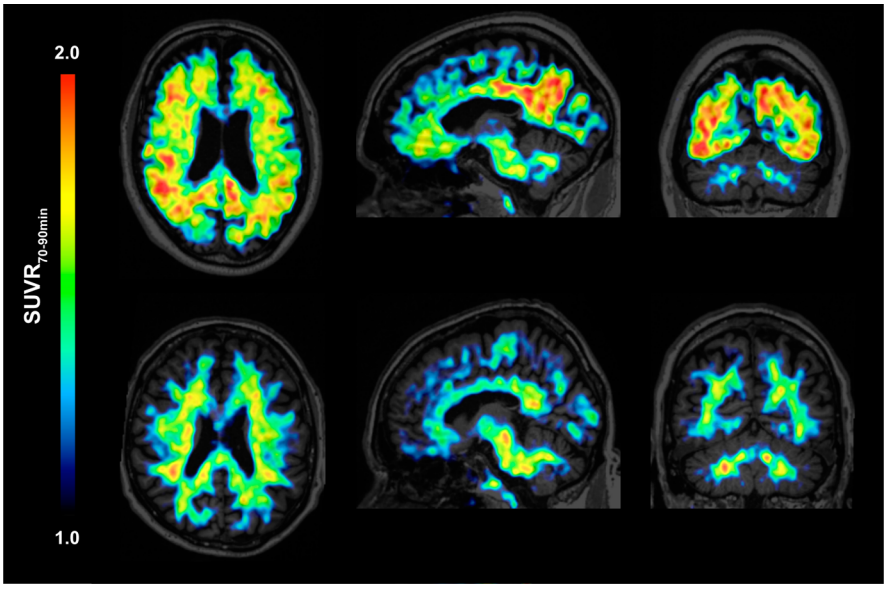

Figure 7. First human brain PET/MR images with [^{18}F]FIBT. PET images of a patient with moderate Alzheimer's disease (top) and a subject defined as control (psychometric testing within normal limits, normal FDG PET, and normal CSF τ, τ*, and Aβ_{1-42} levels) (bottom) coregistered to their corresponding T1-weighted MPRAGE MR images as taken with the Siemens Biograph in a fully dynamic 90 min PET/MR study. 70−90 min postinjection frames are shown as axial (left), sagittal (middle), and coronal (right) views. PET data was transformed to standardized uptake value ratios (SUVRs) using the cerebellum as reference region (scale on left side). Images from the patient with tracer distribution typical for AD (top) show strong contrast to images from the subject (bottom) who was cleared of any signs of neurodegeneration with a tracer distribution typical for healthy controls. Vertical color bar indicates look-up-table "Cold" (taken from Pmod) between ratio values of 1.0 (i.e., equality) and 2.0.

Also, Figure 6A depicts how [^{18}F]FIBT autoradiographs yielded with freshly deparaffinized tissue (as done for [^{11}C]PiB) usually did not show this kind of binding to rim and vessel. This nonspecific binding is most likely due to the tissue being used for in vitro incubation for a second time with dry storage in a fridge in between.

FIBT Correspondence to Amyloid and Tau Immunohistochemistry. While Figure 5 shows [^{18}F]FIBT binding in relation to [^{11}C]PiB, Figure 6 describes its correspondence to binding of standard neurohistology antibodies for Aβ (clone 4G8) and τ (clone AT8). In general, the results confirmed specific and exclusive binding of [^{18}F]FIBT to amyloid depositions. Figure 6 shows conventional plate autoradiography of [^{18}F]FIBT on a temporal cortex section of a severely affected AD patient (staged as CERAD-C, Braak & Braak V). Magnification panels show 4G8 and AT8 micrographs coregistered to the autoradiography on the same section with strong correspondence of [^{18}F]FIBT uptake and 4G8 binding and no common binding with AT8. All [^{18}F]FIBT uptake is localized at Aβ accumulations. On the other hand, some diffuse Aβ plaques as detected by 4G8 did not give

DOI: 10.1021/cn5001827
ACS Chem. Neurosci. 2015, 6, 428−437

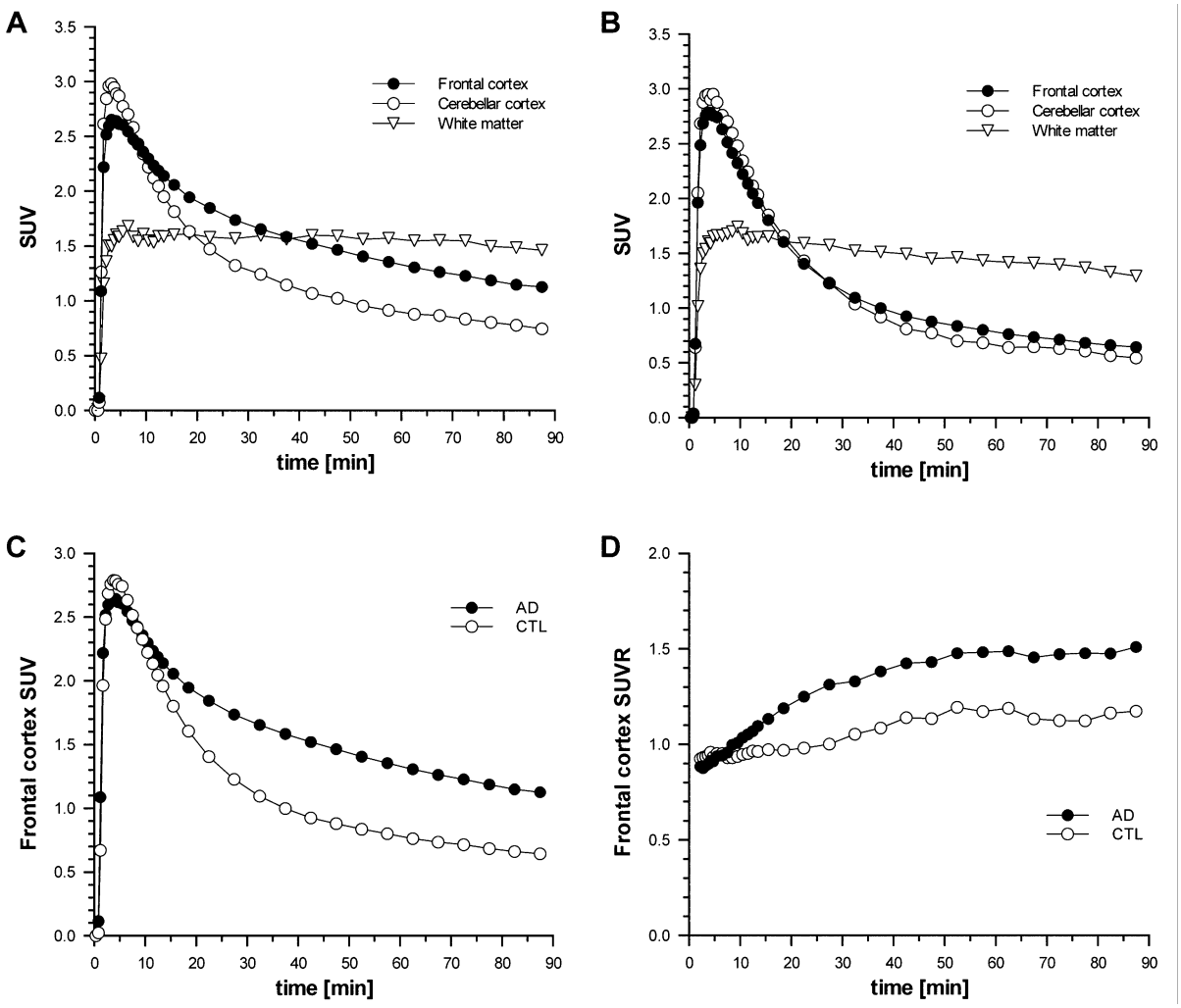

Figure 8. Individual time−activity curves (TACs) for [^{18}F]FIBT in AD patient and control subject. Dynamic 90 min PET study as shown statically over 70−90 min in Figure 7 was reconstructed into 37 frames (4 × 15 s, 8 × 30 s, 9 × 60 s, 2 × 180 s, 14 × 300 s). For retrieval of TACs, three regions were manually defined for each subject: full frontal and cerebellar cortex as well as semioval center representing white matter. Top panels show TACs for AD patient (A) and control subject (B) after transforming calibrated uptake into SUVs. TACs for frontal cortex as shown in panels (A) and (B) are presented together in panel (C) for better comparability. Dynamic ratio development (SUVRs) for frontal cortex relative to cerebellar cortex is shown in panel (D) for both subjects. Data points are located in the middle of each frame.

[^{18}F]FIBT signals. Panels A_4 and B_4 are shown in Supporting Information Figure 2 in the context of larger fields around them.

As for [^{11}C]PiB, [^{18}F]FIBT in vitro binding on human tissue was always correlating to 4G8-positivity (Figure 6A). However, not all 4G8 signals were translated into [^{18}F]FIBT (or equally into [^{11}C]PiB) signals in this autoradiographic method. Binding was related to density of Aβ plaques showing a strong signal for compact cored plaques but a faint or no signal for less compact diffuse or perivascular plaques.

First Human PET with [^{18}F]FIBT. PET imaging results of the first [^{18}F]FIBT administration to two human subjects are presented, here. A 59 year old male patient ("subject-1") was referred to our clinic with the diagnosis of probable moderate dementia due to AD and an MMSE score of 8 as well as a 72 year old male memory complainer ("subject-2") whose diagnostic evaluation yielded a normal range on every subtest of the CERAD-NAB, normal tracer uptake in FDG PET, and normal τ, phosphorylated τ, and Aβ_{1-42} levels in CSF. Therefore, subject-2 was finally diagnosed to be free of neurodegenerative diseases and his [^{18}F]FIBT imaging results were considered as control for this study.

Subject-1 received 200 MBq and subject-2 received 250 MBq of [^{18}F]FIBT intravenously to perform a dynamic 90 min Siemens Biograph PET/MR study each. Figure 7 shows static PET summation frames (70−90 min) of the final 20 min of the PET/MR investigation as SUVR images using the cerebellum as reference region coregistered to the simultaneously acquired MR images.

Visually, [^{18}F]FIBT patient images in top panels showed strong signal resembling known tracer distribution patterns of Aβ radiopharmaceuticals in patients with AD (strong retention in posterior cingulate cortex, precuneus, parietal, temporal, frontal, and occipital cortex) and, thus, confirmed the clinical diagnosis of a probable AD process. In clear contrast, images in bottom panels showed a distribution pattern similar to established Aβ imaging findings in healthy controls free of Aβ pathology (predominantly unspecific white matter uptake and no relevant cortical tracer retention) and, thus, also confirmed the clinical findings and fluid analytes which could not reveal any sign of neurodegenerative disease.

Standardized uptake value ratios (SUVRs) for the same time frame visually shown in Figure 7 (70−90 min) were selected as

DOI: 10.1021/cn5001827
ACS Chem. Neurosci. 2015, 6, 428−437

measures for a first analysis and calculated for all four brain lobes without differentiation between gray and white matter. Reference region definition followed convention and used AAL atlas volume-of-interest definition.[15] This resulted in lobe-wise $SUVRs_{70-90\ min}$ for AD (subject-2 shown in brackets) as frontal 1.81 (1.48), parietal 1.84 (1.47), temporal 1.87 (1.45), and occipital 1.91 (1.52).

Successful finalization of comprehensive [^{18}F]FIBT characterization including in vivo proof-of-principle PET in transgenic mice[8] led to the first in vivo [^{18}F]FIBT PET in a patient with typical AD and a subject without signs of neurodegenerative disease. A good diagnostic Aβ radiopharmaceutical should enable easy and specific clinical diagnosis through strong image signal and high image contrast such that even laymen could make at least a binary diagnosis regarding presence of health or disease. Figure 7 shows human [^{18}F]FIBT PET images (using 70−90 min static frames) that probably fulfill these requirements. SUVRs are increasingly judged to be of limited value for disease staging.[16] Still, the ease in yielding these ratios makes them common and helpful measures. In analogy to the visual signal, lobewise [^{18}F]FIBT SUVRs of the case presented here compared well to SUVRs of Aβ PET tracers like [^{11}C]PiB.[17]

Static [^{11}C]PiB images are often taken for 40−70 min in clinical settings. These short postdose waiting periods of 0.5 h would be possible for [^{18}F]FIBT to provide well readable images. However, [^{18}F]FIBT pharmacokinetics are slower than [^{11}C]PiB kinetics, and different summation protocols up to 90 min suggested higher contrast images toward later time frames.

Occipital uptake in the AD patient was slightly higher than expected but not unusually high. It may be indicative of cerebral amyloid angiopathy (CAA) to follow at later stages.[18] At this stage, none of our patients showed intracerebral hemorrhages and the amount of microhemorrhages seen in gradient echo sequences varied between 0 and 1 (data not shown). Thus, comorbid CAA was likely not present.

For reading out representative time-activity curves (TACs), volumes-of-interest were manually defined for frontal cortex, cerebellar cortex, and semioval center for each subject in analogy to a report on Florbetaben.[19] Figure 8 shows the results for the 90 min scan duration after data was transformed to SUV for better comparability of both subjects. Flushing of [^{18}F]FIBT into frontal and cerebellar cortex peaked around 3 min p.i. for both subjects and initial uptake into cerebellum was always higher. For the AD patient, uptake in frontal cortex clearly went above cerebellar uptake around 10 min p.i. while this separation not only happened nearly 20 min later in the control subject but the frontal cortex uptake stayed close to cerebellar uptake. A direct comparison of frontal cortex uptake (Figure 8C) similarly showed that curve behavior distinguished AD from control within 10 min p.i. and that frontal cortical tissue of the control subject washed out considerably faster. Figure 8D provides another representation by showing dynamic frontal cortex SUVRs for both individuals which separate around 10 min p.i.

The clinical feasibility of [^{18}F]FIBT for good PET image readouts described above was further supported by extracting dynamic SUVs (Figure 8). Strong image signal and high image contrast reflected good curve contrast, that is, sufficient tracer retention in target-rich tissue relative to reference tissue in the AD patient and good washout behavior in the control subject. Comparing individual SUV behavior over time with published data for Florbetaben[19] indicated that [^{18}F]FIBT may compare well to established fluorinated Aβ PET ligands like Florbetaben.

CONCLUSION

The ^{18}F-fluorinated imidazo[2,1-*b*]benzothiazole [^{18}F]FIBT was characterized comprehensively. Its preferable properties as a PET tracer were shown in vitro and ex vivo using human and rodent brain material in comparison to PiB leading to its first and very encouraging use in humans. [^{18}F]FIBT is a promising next-generation diagnostic Aβ radiopharmaceutical and robust imaging tool with potential to become an AD biomarker. It compares well to existing Aβ PET ligands and hence motivates further human investigations probably including dementia entities other than Alzheimer's disease.

METHODS

Human Subjects. The study was performed in accordance with German Medicinal Product Act (Arzneimittelgesetz) and German Radiation Safety Act (Strahlenschutzverordnung). Retrospective analyses and publication of data were approved by the local ethics committee.

Two human subjects were recruited from the outpatient memory clinic of the Department of Psychiatry and Psychotherapy at Technische Universität München (TUM). They had been referred for diagnostic evaluation of cognitive impairment and underwent a standardized diagnostic protocol. Examinations were part of their routine checkup in the course of the evaluation of the patient's suspected neurodegenerative disorders. Psychometric workup was based on the Consortium to Establish a Registry for AD Neuropsychological Assessment Battery (CERAD-NAB), which includes the Mini-Mental-State Examination (MMSE). All patients provided written informed consent regarding scientific evaluation of their data.

Animals. All experiments except toxicity studies were carried out with the approval of the institutional animal care committee of the District Government of Upper Bavaria in Munich, Germany, and in accordance with German Animal Welfare Act. Animal husbandry followed regulations of European Union guideline no. 2010/63.

These experiments were performed in homozygous APP/PS1 mice (B6;CB-Tg(Thy1-PSEN1*M146 V/Thy1-APP*swe)-10Arte) (TaconicArtemis, Cologne, Germany) on a congenic C57BL/6J genetic background and commercially available age- and gender-matched controls (Harlan-Winkelmann, Borchen, Germany and Janvier, Le Genest-St-Isle, France) in addition to commercially available male Balb-C mice and male Swiss-Webster rats (both from Charles River Laboratories, Sulzfeld, Germany). The transgenic mouse model has profoundly been characterized regarding onset, progression, distribution, and extent of Aβ plaque deposition as well as behavioral features and its potential for PET imaging.[9,11]

An acute single dose toxicity study was performed at Harlan Laboratories, Itingen, Switzerland, in compliance with Swiss Ordinance relating to Good Laboratory Practice, adopted May 18th, 2005 [SR 813.112.1]. It is based on OECD Principles of Good Laboratory Practice as of November 26th, 1997 [C(97)186/Final]. These principles are compatible with Good Laboratory Practice regulations specified by regulatory authorities throughout the European Community and the United States (EPA and FDA).

Two groups of three female Harlan:NMRI (SPF) mice each ("group 1" and "group 2") were used for this study during which the animals were given free access to food and water at all times.

ASSOCIATED CONTENT

Supporting Information

Experimental protocols and material applied for this study. This material is available free of charge via the Internet at http://pubs.acs.org.

DOI: 10.1021/cn5001827
ACS Chem. Neurosci. 2015, 6, 428−437

AUTHOR INFORMATION

Corresponding Author

*Mailing address: Department of Pharmaceutical Radiochemistry, Technische Universität München, Walter-Meissner Strasse 3, 85748 Garching, Germany. Phone: + 49 89 289 10265. Fax: + 49 89 289 10204. E-mail: b.yousefi@tum.de.

Author Contributions

#B.H.Y. and A.M. contributed equally.

Funding

Research leading to results presented in this work has received funding from Deutsche Forschungsgemeinschaft (DFG, German Research Foundation, Grant Code HE4560/1-3) and the Research Training Group 1373.

Notes

The funders had no role in study design, data collection and analysis, decision to publish, or preparation of the manuscript. The authors declare no competing financial interest.

ACKNOWLEDGMENTS

We would like to thank Axel Walch and Bernhard Hemmer for granting access to their facilities and Heinz von der Kammer and Michael Schoor for providing the transgenic APP/PS1 animal model. We are grateful to Monika Beschorner, Sybille Reder, Frauke Hoffmann, Annette Frank and Martina Weineisen for excellent technical assistance in the lab and we very much appreciate the scientific collaboration with Lucas Martin and Sabine Krause for estimation of ligand specificity.

REFERENCES

(1) Henriksen, G., Yousefi, B., Drzezga, A., and Wester, H.-J. (2008) Development and evaluation of compounds for imaging of β-amyloid plaque by means of positron emission tomography. *Eur. J. Nucl. Med. Mol. Imaging 35*, 75−81.

(2) Agdeppa, E. D., Kepe, V., Liu, J., Flores-Torres, S., Satyamurthy, N., Petric, A., Cole, G. M., Small, G. W., Huang, S. C., and Barrio, J. R. (2001) Binding characteristics of radiofluorinated 6-dialkylamino-2-naphthylethylidene derivatives as positron emission tomography imaging probes for beta-amyloid plaques in Alzheimer's disease. *J. Neurosci. 21* (24), RC189.

(3) Noda, A., Murakami, Y., Nishiyama, S., Fukumoto, D., Miyoshi, S., Tsukada, H., and Nishimura, S. (2008) Amyloid imaging in aged and young macaques with [11C]PIB and [18F]FDDNP. *Synapse 62* (6), 472−475.

(4) Mathis, C. A., Wang, Y., Holt, D. P., Huang, G. F., Debnath, M. L., and Klunk, W. E. (2003) Synthesis and evaluation of 11C-labeled 6-substituted 2-arylbenzothiazoles as amyloid imaging agents. *J. Med. Chem. 46* (13), 2740−2754.

(5) Small, G. W., Kepe, V., Ercoli, L. M., Siddarth, P., Bookheimer, S. Y., Miller, K. J., Lavretsky, H., Burggren, A. C., Cole, G. M., Vinters, H. V., Thompson, P. M., Huang, S. C., Satyamurthy, N., Phelps, M. E., and Barrio, J. R. (2006) PET of brain amyloid and tau in mild cognitive impairment. *N. Engl. J. Med. 355* (25), 2652−2663.

(6) (a) Kung, M. P., Hou, C., Zhuang, Z. P., Cross, A. J., Maier, D. L., and Kung, H. F. (2004) Characterization of IMPY as a potential imaging agent for beta-amyloid plaques in double transgenic PSAPP mice. *Eur. J. Nucl. Med. Mol. Imaging 31* (8), 1136−1145. (b) Kung, M. P., Hou, C., Zhuang, Z. P., Zhang, B., Skovronsky, D., Trojanowski, J. Q., Lee, V. M., and Kung, H. F. (2002) IMPY: an improved thioflavin-T derivative for in vivo labeling of beta-amyloid plaques. *Brain Res. 956* (2), 202−210.

(7) Yousefi, B. H., Manook, A., Drzezga, A., von Reutern, B., Schwaiger, M., Wester, H. J., and Henriksen, G. (2011) Synthesis and evaluation of 11C-labeled imidazo[2,1-b]benzothiazoles (IBTs) as PET tracers for imaging beta-amyloid plaques in Alzheimer's disease. *J. Med. Chem. 54* (4), 949−956.

(8) Yousefi, B. H., Drzezga, A., Reutern, B. v., Manook, A., Schwaiger, M., Wester, H.-J. r., and Henriksen, G. (2011) A novel 18F-labeled imidazo[2,1-b]benzothiazole (IBT) for high-contrast PET imaging of β-amyloid plaques. *ACS Med. Chem. Lett. 2* (9), 673−677.

(9) Manook, A., Yousefi, B. H., Willuweit, A., Platzer, S., Reder, S., Voss, A., Huisman, M., Settles, M., Neff, F., Velden, J., Schoor, M., von der Kammer, H., Wester, H. J., Schwaiger, M., Henriksen, G., and Drzezga, A. (2012) Small-animal PET imaging of amyloid-beta plaques with [11C]PiB and its multi-modal validation in an APP/PS1 mouse model of Alzheimer's disease. *PLoS One 7* (3), e31310.

(10) Irwin, D. J., Lee, V. M., and Trojanowski, J. Q. (2013) Parkinson's disease dementia: convergence of alpha-synuclein, tau and amyloid-beta pathologies. *Nat. Rev. Neurosci. 14* (9), 626−636.

(11) Willuweit, A., Velden, J., Godemann, R., Manook, A., Jetzek, F., Tintrup, H., Kauselmann, G., Zevnik, B., Henriksen, G., Drzezga, A., Pohlner, J., Schoor, M., Kemp, J. A., and von der Kammer, H. (2009) Early-onset and robust amyloid pathology in a new homozygous mouse model of Alzheimer's disease. *PLoS One 4* (11), e7931.

(12) von Reutern, B., Grunecker, B., Yousefi, B. H., Henriksen, G., Czisch, M., and Drzezga, A. (2013) Voxel-Based Analysis of Amyloid-Burden Measured with [(11)C]PiB PET in a Double Transgenic Mouse Model of Alzheimer's Disease. *Mol. Imaging Biol. 15* (5), 576−584.

(13) Johnston, M., Zakharov, A., Papaiconomou, C., Salmasi, G., and Armstrong, D. (2004) Evidence of connections between cerebrospinal fluid and nasal lymphatic vessels in humans, non-human primates and other mammalian species. *Cerebrospinal Fluid Res. 1* (1), 2.

(14) Klunk, W. E., Lopresti, B. J., Ikonomovic, M. D., Lefterov, I. M., Koldamova, R. P., Abrahamson, E. E., Debnath, M. L., Holt, D. P., Huang, G. F., Shao, L., DeKosky, S. T., Price, J. C., and Mathis, C. A. (2005) Binding of the positron emission tomography tracer Pittsburgh compound-B reflects the amount of amyloid-beta in Alzheimer's disease brain but not in transgenic mouse brain. *J. Neurosci. 25* (46), 10598−10606.

(15) Tzourio-Mazoyer, N., Landeau, B., Papathanassiou, D., Crivello, F., Etard, O., Delcroix, N., Mazoyer, B., and Joliot, M. (2002) Automated anatomical labeling of activations in SPM using a macroscopic anatomical parcellation of the MNI MRI single-subject brain. *NeuroImage 15* (1), 273−289.

(16) Ikoma, Y., Edison, P., Ramlackhansingh, A., Brooks, D. J., and Turkheimer, F. E. (2013) Reference region automatic extraction in dynamic [(11)C]PIB. *J. Cereb. Blood Flow Metab. 33* (11), 1725−1731.

(17) Lopresti, B. J., Klunk, W. E., Mathis, C. A., Hoge, J. A., Ziolko, S. K., Lu, X., Meltzer, C. C., Schimmel, K., Tsopelas, N. D., DeKosky, S. T., and Price, J. C. (2005) Simplified quantification of Pittsburgh Compound B amyloid imaging PET studies: a comparative analysis. *J. Nucl. Med. 46* (12), 1959−1972.

(18) Johnson, K. A., Gregas, M., Becker, J. A., Kinnecom, C., Salat, D. H., Moran, E. K., Smith, E. E., Rosand, J., Rentz, D. M., Klunk, W. E., Mathis, C. A., Price, J. C., Dekosky, S. T., Fischman, A. J., and Greenberg, S. M. (2007) Imaging of amyloid burden and distribution in cerebral amyloid angiopathy. *Ann. Neurol. 62* (3), 229−234.

(19) Barthel, H., Luthardt, J., Becker, G., Patt, M., Hammerstein, E., Hartwig, K., Eggers, B., Sattler, B., Schildan, A., Hesse, S., Meyer, P. M., Wolf, H., Zimmermann, T., Reischl, J., Rohde, B., Gertz, H. J., Reininger, C., and Sabri, O. (2011) Individualized quantification of brain beta-amyloid burden: results of a proof of mechanism phase 0 florbetaben PET trial in patients with Alzheimer's disease and healthy controls. *Eur. J. Nucl. Med. Mol. Imaging 38* (9), 1702−1714.

DOI: 10.1021/cn5001827
ACS Chem. Neurosci. 2015, 6, 428−437